Entry, Descent, and Landing GN&C System Evaluation via Cable-Driven Emulation Robotics

Davis Weaver Adams*, Teming Tse†, Sean Downs‡, Ronald Sostaric §, Joshua Sooknanan ¶ and Derek Bankieris ‖
NASA Johnson Space Center, Houston, TX 77058

Caleb Peck ** and Manoranjan Majji††
Texas A&M University, College Station, TX, 77840

Hector Li Sanchez, M. Ebrahim Mohammadi, Ringnyu Bunji Antoinette, James Walton and Chris Owens
Astrobotic Technology, Pittsburgh, PA 15233

An innovative cable-driven parallel robot named the Six Degree-of-Freedom Tendon Actuated Robot (STAR), recently developed by researchers at NASA Johnson Space Center, was built to enable entry, descent, and landing (EDL) emulation experiments. Upon functional testing and system verification, STAR employed several simulated EDL trajectories to validate velocimeter LIDAR-based sensor models for cooperative terrain relative navigation applications for its first testing campaign. The STAR lab also hosted researchers from Astrobotic to evaluate the real-time performance of a newly developed sensor payload, UltraNav, through hardware in-the-loop-testing (HWIL). This work introduces the STAR system along with its accompanying testing utilities and capabilities, and deliver the experimental methodology and results of test campaigns performed with the STAR facility to date.

I. Introduction

Spaceflight is expensive, often precluding low-TRL testing of spacecraft to be performed in zero- or micro-gravity. This creates a need for platforms that emulate the space environment to assess the performance of GN&C algorithms and validate the robustness of these algorithms prior to launch. Due to the unique, "one-off" nature of spacecraft missions, test environments are typically created for specific procedures as opposed to the entire mission design. For example, the NASA Neutral Buoyancy Laboratory near Johnson Space Center (JSC) is one of the world's largest pools that allows astronaut trainees to develop their skills in a pseudo-zero gravity environment [1]. The Space Power Facility at NASA Glenn Research Center is a large vacuum chamber that allows for full scale hardware and software testing in an emulated space environment, such as full-scale rocket-fairing separation tests, Mars Lander system tests, deployable solar sail and solar array tests, International Space Station (ISS) radiator deployment tests, and high-energy experiments [2]. Spacecraft GN&C system performance can be evaluated in a laboratory environment via emulation robotics platforms. There is no 'perfect' motion emulation environment, which means that different platforms are best suited for different motion emulation projects. Notable existing emulation robotics facilities include the Formation Control Testbed (FCT) (or "Robodome") at NASA Jet Propulsion Laboratory [3], the Active Response Gravity Offload System (ARGOS) at NASA JSC [4], and Texas A&M's Land, Air, and Space Robotics (LASR) Laboratory. The FCT is mainly utilized for developing autonomous guidance, navigation, and control (GN&C) algorithms related to precision formation flight. ARGOS was designed to emulate reduced gravity environments as a training and evaluation tool for prospective astronauts. The LASR Laboratory at Texas A&M University hosts a suite of motion emulation robots for various rendezvous, proximity operations, and docking (RPOD) missions [5, 6]. Each of these emulation robotics facilities provide an excellent platform for GN&C system development and validation within the scope of their original purpose. However, one particularly challenging spacecraft relative navigation operation to emulate is entry, descent, and

*Navigation Engineer, Aeroscience and Flight Mechanics Division, davis.w.adams@nasa.gov
†Navigation Engineer, Aeroscience and Flight Mechanics Division, teming.tse-1@nasa.gov
‡Navigation Engineer, Aeroscience and Flight Mechanics Division, sean.p.downs@nasa.gov
§SPLICE Project Manager, Aeroscience and Flight Mechanics Division, ronald.r.sostaric@nasa.gov
¶Robotics Engineer, Robotics Division, josh.sooknanan@nasa.gov
‖Robotics Engineer, Robotics Division, derek.r.bankieris@nasa.gov
**Graduate Research Assistant, Department of Aerospace Engineering, Texas A&M University, cpeck7@tamu.edu
††Assistant Professor, Director, LASR Laboratory, Department of Aerospace Engineering, AIAA Associate Fellow, mmajji@tamu.edu

landing (EDL) scenarios due to many factors including size, weight, and power (SWAP) considerations and trajectory scale.

The Six Degree-of-Freedom Tendon Actuated Robot (STAR), shown in Fig. 1, is a new motion emulation platform developed at NASA JSC for the Safe and Precise Landing Integrated Capabilities Evolution (SPLICE) project to enable EDL and RPOD emulation experiments as a means to validate and evaluate the performance of relative navigation algorithms [7, 8]. STAR provides smooth rigid body motion through eight cables attached to powerful stagnant winches placed in the corners of a rectangular frame. Each winch consists of a large DC motor to actuate the cable, absolute encoders to track the cable lengths, force transducers to monitor cable tension, a cable drum to prevent cable knots, and accompanying electronics. The platform is capable of supporting a payload of up to 50 kg and implementing trajectories within the 7mx10mx7m (LxWxH) volume with a maximum translation velocity of 2 m/s, translational acceleration of 1 m/s^2, and rotational deflection of $\pm 10°$in all axes. Based on the desired instantaneous configuration of the payload, STAR's internal controller solves the inverse kinematics problem to generate appropriate cable lengths and retraction rates. Therefore, arbitrary time-varying position and orientation trajectories within the limits of the robot can be implemented with ease.

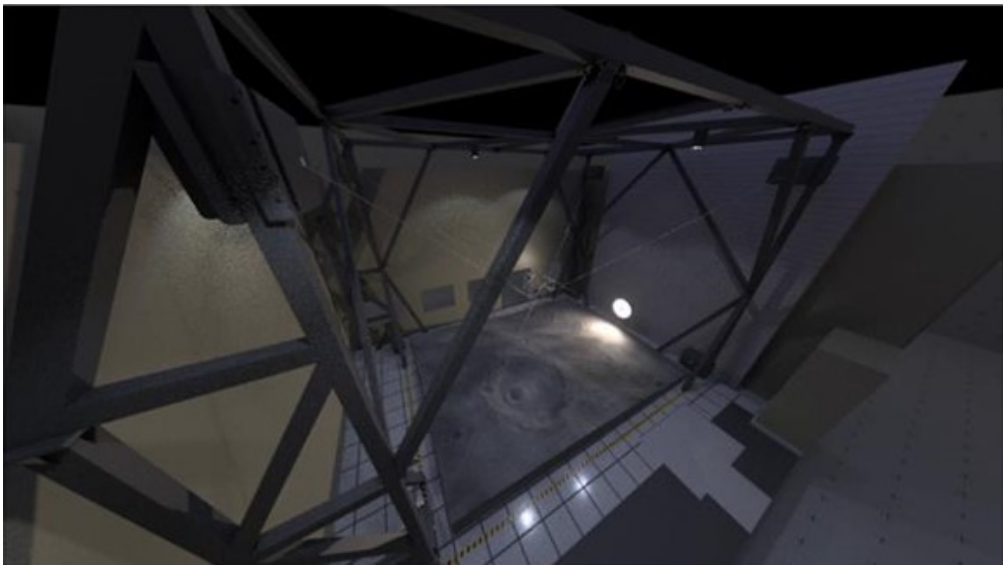

Fig. 1 Model of Six Degree-of-Freedom Tendon Actuated Robot (STAR)

The first test campaign of this new platform was designed to validate and evaluate the performance of point-wise relative position and Doppler velocity measurement models in the context of a multiplicative extended Kalman filter (MEKF). During cooperative terrain relative navigation (TRN), it is assumed that observed features can be associated with features stored in an on-board map resulting in the true locations of the feature expressed in a local terrain frame. This information substantially improves a navigation system's capability to estimate the complete pose of the spacecraft in highly dynamic and uncertain conditions as compared to a system solely comprised of inertial sensors. Inclusion of a point-wise relative Doppler velocity measurement obtained by a novel velocimeter light detection and ranging (LIDAR) sensor further refines this pose estimate and increases the confidence of the resultant solution. This information, combined with data streams from a gyroscope and accelerometer, is fused within a MEKF architecture resulting in a comprehensive relative navigation solution [9]. The second STAR laboratory test campaign was developed to perform HWIL testing of Astrobotic's Ultra-Compact Standalone Visual Relative Navigation system, UltraNav. Astrobotic has been evolving UltraNav under NASA's Small Business Innovation Research (SBIR) Phase II award since 2020 and has recently undertaken functional and verification testing for the system. The goal of this test campaign was to evaluate UltraNav's efficacy with regards to 2D feature recognition, characterization, and correspondence in a real time dynamic environment as well as the accuracy of the final pose estimate yielded by the proprietary navigation algorithm.

This work will first introduce the STAR platform. The structural design, end-effector mechanics, and control methodology will be discussed in detail. Then, the STAR laboratory testing utilities will be discussed and the experimental methodology and results of testing campaigns performed with the STAR facility to date will be presented. Finally, potential use cases of the STAR facility will be proposed for future endeavors.

II. Six-Degree of Freedom Tendon Actuated Robot Overview

The STAR is a large-format 6 degree-of-freedom motion platform. The working envelope of the machine is approximately 7m wide × 10m long × 7m tall. The desired performance capabilities of the STAR are a translational velocity of 2 m/s, an acceleration capability of 1 m/s^2, and a rotational capability of ± 10°. A CAD model of the STAR is shown in Fig. 2 below.

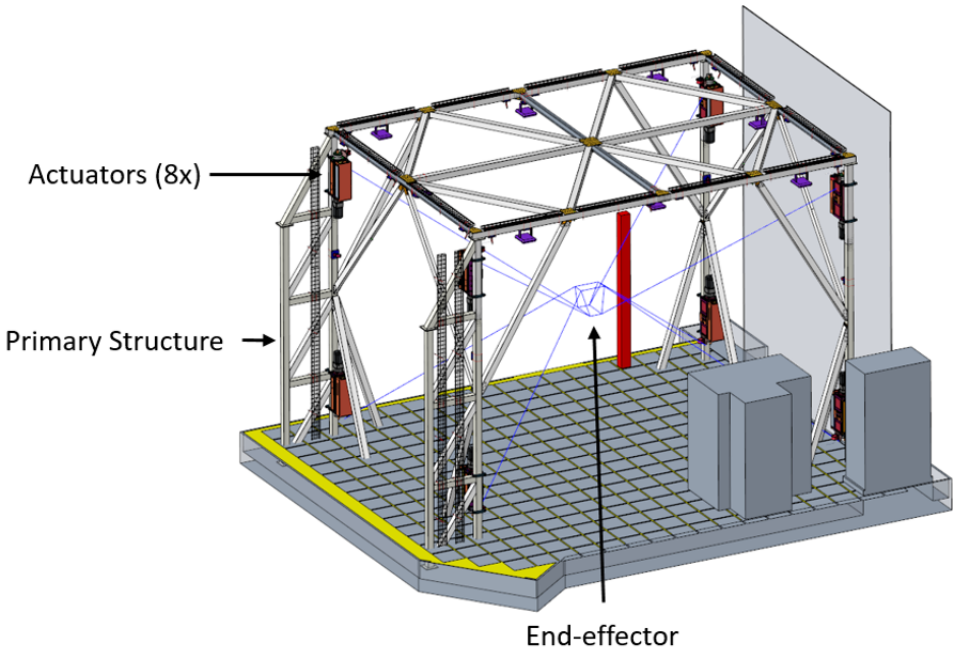

Fig. 2 Computer aided design (CAD) model of STAR infrastructure

The STAR system is modelled after a tendon actuated Stewart-Gough platform, a type of parallel robot utilizing multiple identical actuators to afford six degree-of-freedom motion. The STAR system utilizes eight identical robotic winches attaching to a central end-effector in a parallel configuration, forming a machine commonly known as a cable-driven parallel robot. Using a configuration of four winches on the top of the structure and four winches on the bottom of the structure, the end-effector can translate and rotate within the primary structure of the robot. The STAR system uses 5mm diameter tendons, or cables, made from a synthetic material called Dyneema rather than steel braids. Using synthetic cables reduces the inertia of the system and is stiffer than the equivalent diameter steel cable. The Dyneema cable does not appreciably stretch under load which improves controllability of the system as well as reduces the potential for cables whip in the event of a cable failure. The eight winches on the STAR are capable of sourcing up to 20kW of power continuously and generating up to 1,800lbf of cable tension each. The high-power nature of the machine affords stable operation with a variety of payload configurations while maintaining a large workspace.

A. Robot Design

The primary structure, shown in Fig. 2, is responsible for supporting each of the eight actuators, facility lighting, facility cameras supporting operator awareness, motion tracking cameras, and all static electronic cables. The primary structure is constructed of a mixture of steel and aluminum beams and weldments. The structure is designed with a first mode natural frequency of 9Hz to ensure control stability of the machine. The total tension load of 1,800lbf from each actuator location, totaling in 14,400lbf, was used as a design parameter when determining the geometry.

The actuator, or winch, is used to actuate the tendons of the STAR. These tendons apply force to the end-effector of the robot to achieve an arbitrary pose within the operational envelope of the robot. The STAR winch is shown in Fig. 3. Each winch is a self-contained robotic system and houses its own electronics. As such, the winch assembly only requires connections for power and communication. The winch utilizes heritage design concepts from the Active Response Gravity Offload System (ARGOS), also found at the Johnson Space Center. The winch uses a traversing drum

to ensure stable tracking of cable length and repeatable cable winding within the winch. Kollmorgen motor and drive components are utilized. Sensors include end-of-travel limit switches, a linear laser encoder to verify internal drum position, an absolute position rotary encoder to track cable length, and a proximal load cell to measure cable tension.

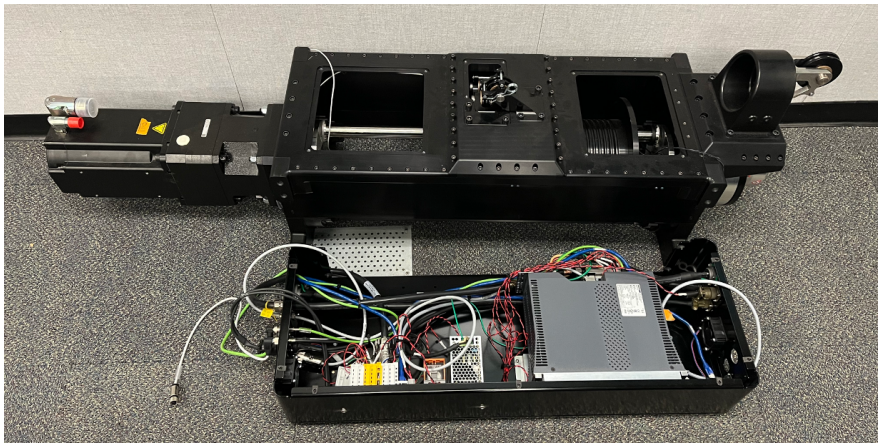

Fig. 3 STAR winch

The STAR end-effector, displayed in Fig. 4, is an aluminum weldment that is powder coated black to minimize interference with simulated lighting and motion tracking sensors. Similar to the primary structure, the end-effector was designed using the 1,800lbf tension capability of the actuators to ensure adequate strength and stiffness. The tendons attach to high-strength rod-ends at the corners of the end-effector to ensure the rotation point of the tendon with respect to the end-effector remains constant throughout the workspace of STAR. The upper and lower corners of the end-effector are in a skewed configuration, which increases the robot's rotational capability and avoids tendon to tendon collisions. The end-effector features optical plates on the top and bottom with vibration isolating mounts for payload interfacing. The end-effector package is also available with internally mounted batteries at several voltage levels to support a wide range of payloads. The tendons attach to rod-ends at the corners of the end-effector to ensure the rotation point of the cable with respect to the end-effector remains the same. The upper and lower corners of the end-effector are in a skewed configuration, which increases the robot's rotational capability.

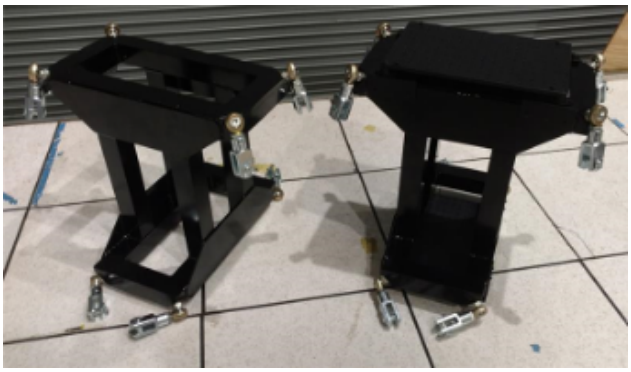

Fig. 4 STAR end-effector (2× shown)

B. Control and Operation

STAR is controlled using an inverse kinematics control architecture. The coordinate frames of the actuators are fixed in space, where as the end-effector desired frame is variable. A visual representation of the coordinate frames is displayed in Fig. 5. The desired end-effector pose is used to estimate the magnitude of vectors from the actuator frames to the end-effector vertex frames. The tendon lengths of the actuators are determined using an absolute position encoder tracking the rotational position of the cable drum. The error in tendon length is sensitive to the calibration of each

actuator which was performed at the time of assembly. This calibration is further refined during installation to STAR by using the proximal load cells featured in each actuator to balance loads across the system.

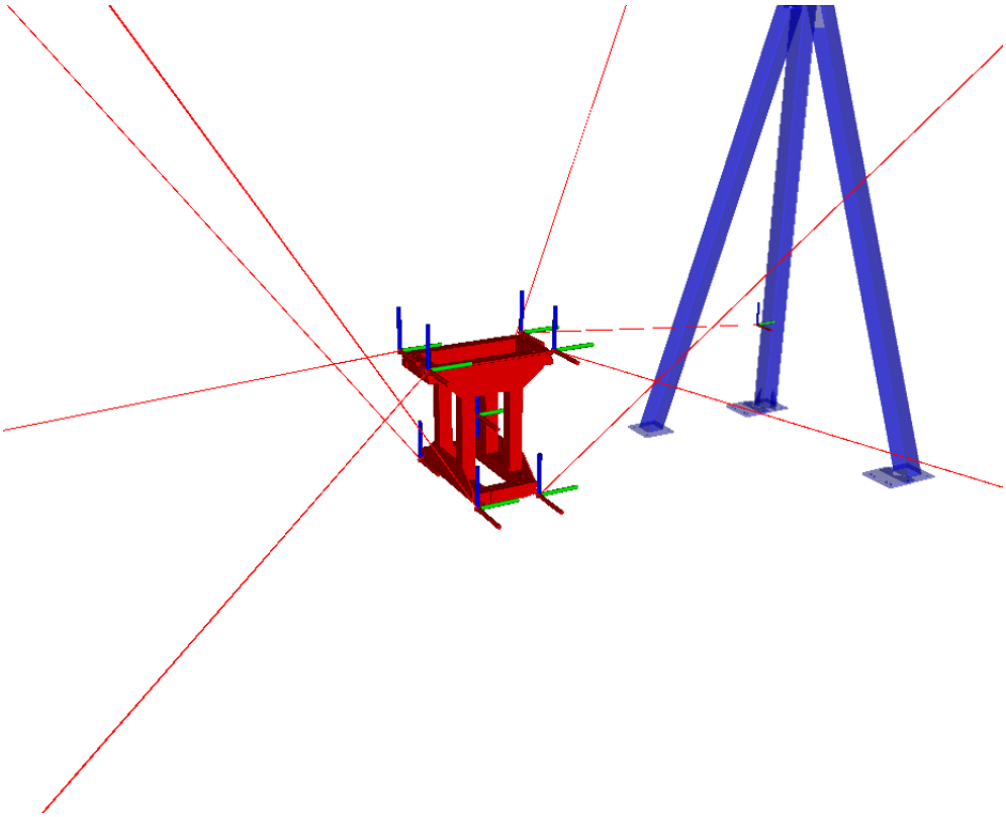

Fig. 5 End-effector coordinate frames and estimated tendon positions

STAR's software architecture was built using Robot Operating System (ROS) tools. ROS is an open source software framework for robot applications including walking robots, robotic arms, wheeled robots, and drones [10]. A preexisting parallel robotics package was not utilized in the development of STAR, however the base set of tools available as part of ROS were instrumental in developing the machine. STAR was developed using ROS Noetic and Ubuntu 20.04LTS. STAR is currently using ROS1 which does not have real-time capabilities as standard. The Linux Low Latency package is used to improve timing and synchronization between nodes and actuators. Alternatively, the PREEMPT_RT kernel patch could be implemented [11]. Eventually, ROS2 will be tested on the STAR platform.

A simplified high-level control flow diagram is shown in Fig. 6. Most of the computation is linear until the trajectory information is sent to each actuator. Timing and coordination between the actuators are critical to ensure smooth operation. Each block in the diagram essentially represents a ROS node. EtherCAT is used to perform low-level communication from actuators to the control computer through a proprietary EtherCAT driver that has been implemented using NASA's open-source Trick software [12]. Feedback control for the actuator is performed in a ROS Node. Commands to the actuators are sent via ROS message and encoded into EtherCAT to control the electric motors. Using ROS tools for prototyping, a constant jerk trajectory generation algorithm was developed. This algorithm generates smooth trajectories for a single actuator and can also be applied to the six degree of freedom motion of the whole robot. A screenshot depicting constant jerk motion is displayed in Fig. 7.

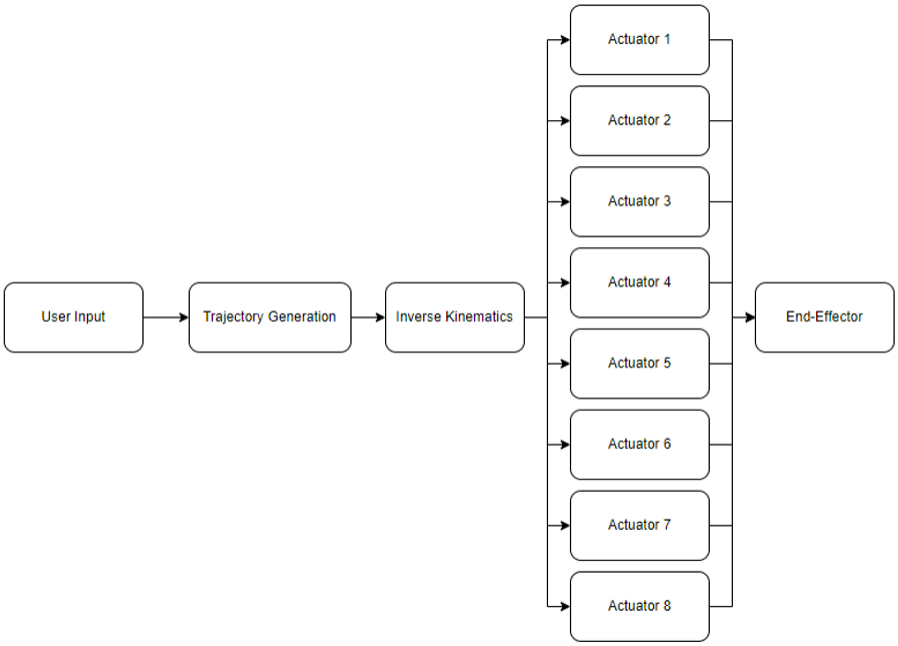

Fig. 6 STAR high-level controller block diagram

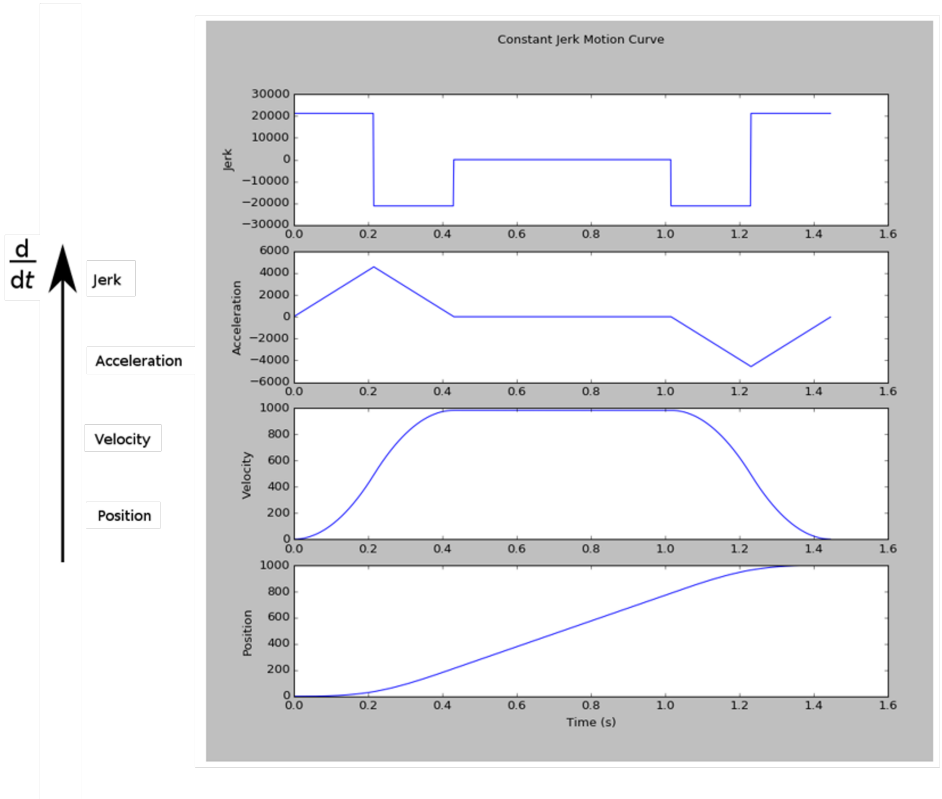

Fig. 7 Constant jerk trajectory generated by STAR trajectory planner

During operation, the STAR is controlled with a custom python-based graphical user interface (GUI), as displayed in Fig. 8. After clearing any faults and enabling the actuators, there are three different operational modes: 1) jog/joystick, 2) set position and 3) point streaming. The jog/joystick mode responds to serial user commands to perform translations along or rotations about any of the three axes. In set position mode, the user commands the robot to move to any desired pose within the robot's operational envelop. Finally, the point streaming mode commands the robot to follow an arbitrary user-defined sequence of poses at various times. Point streaming mode enables open loop spacecraft emulation trajectories to be performed. Embedding closed loop control via point streaming mode is currently under development.

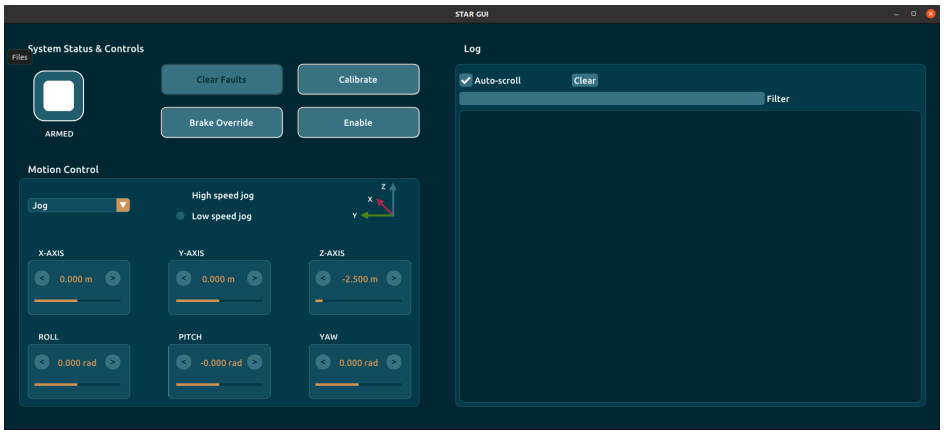

Fig. 8 STAR controller graphical user interface (GUI)

III. STAR Laboratory Experimental Testing

At its core, STAR was designed to emulate any spacecraft in any environment, within the confines of the robot's operational limits. The STAR facility was developed to be a unique hardware in-the-loop test bed to aid in the advancement of precision landing technologies. Specifically, STAR was designed under the SPLICE project umbrella to streamline rapid prototyping and functional testing of the novel Descent and Landing Computer (DLC). A high-level system diagram presenting the STAR facility HWIL emulation testing information flow for SPLICE is displayed in Fig. 9. The purple "spacecraft" block showcases the modular quality of this system since the robot can implement arbitrary trajectories including spacecraft-specific EDL and RPOD scenarios.

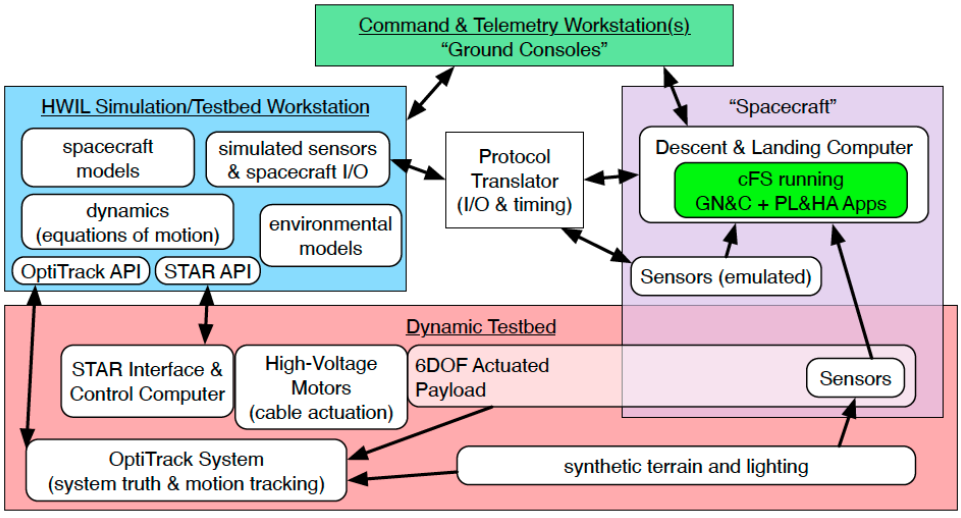

Fig. 9 SPLICE HWIL system diagram from STAR testing

As one of the main purposes of the STAR facility is to enable validation testing of navigation algorithms in a controlled environment, it is vital to have baseline truth data to compare resultant estimates with. The STAR facility is outfitted with Optitrack Motion Capture System to track the motion of the robot and the location of any ground features expressed in a common reference frame. Reference frame calibration must be performed for each payload configuration to determine the homogeneous transformations between the Optitrack body-fixed frame and any sensor reference frames. Then, resultant state estimates produced by the navigation algorithm under test can directly be compared to the Optitrack ground truth data.

Although the original intention of the STAR facility was to aid in the rapid development of the DLC, the novel robot is agnostic to the payload and is adept for testing any GN&C system in a laboratory setting. While external customers can provide proprietary payloads to mount directly the STAR end-effector, an in-house sensor payload was developed to provide a plug-and-play solution for those looking to exclusively test algorithms in a HWIL environment.

A. STAR End-Effector Sensor Payload

The Compact Multi-Modal Attachment for Navigation Data Synthesis (COMMANDS) sensor payload, displayed in Fig. 10 was designed to accommodate wide ranges of spacecraft GN&C algorithm testing. Similar to it's predecessor, Navigation, Estimation, and Sensing Testbed (NEST), COMMANDS consists of a Cepton LIDAR, VectorNav VN-200T IMU, FLIR Blackfly machine vision camera, an Intel NUC, and a cooling fan. All components are housed in a custom aluminum encolsure that mounts directly to the STAR end-effector.

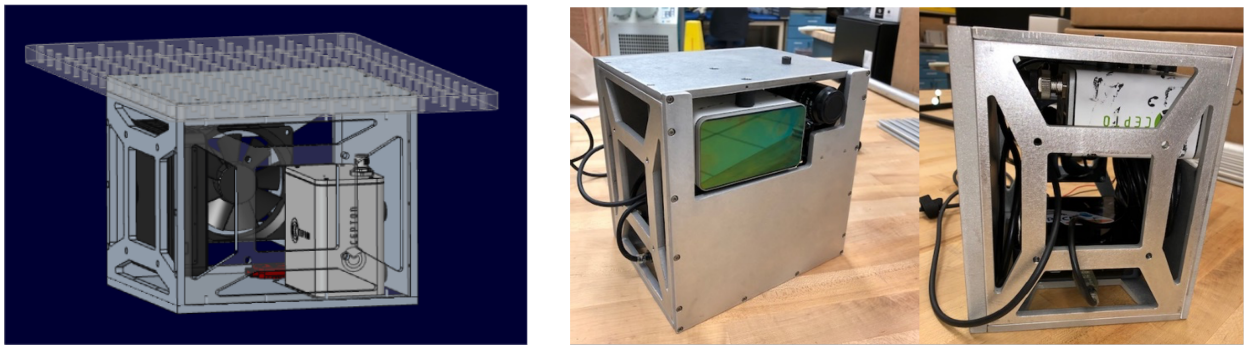

(a) CAD model **(b) Fabricated**

Fig. 10 The Compact Multi-Modal Attachment for Navigation Data Synthesis (COMMANDS) sensor payload

During operation, COMMANDS acquires time-synced data from Optitrack and all of its sensors and live-streams the data over a ROS network. This data can then be leveraged by outer-loop GN&C algorithms to perform the desired experimental test. The homogeneous transformations mapping each of the sensor reference frames to one another were obtained through a rigorous calibration procedure. A partial-update Schmidt MEKF was employed to process the COMMANDS data produced during a calibration test [13]. This calibration provides confident estimates for the position and attitude lever arms from the IMU to the camera and LIDAR. The trajectory that STAR implemented for this calibration procedure was designed to excite every axis of the accelerometer and gyroscope. The trajectory is displayed in Fig. 11 and the underlying translational and angular velocities of the profile are displayed in Fig. 12. The origin of STAR's operational reference frame lies in the center of the workspace. Therefore, the robot can achieve arbitrary poses within $x \in [-3m, 3m]$, $y \in [-4m, 4m]$ and $z \in [-3m, 3m]$ where the z-axis is the vertical direction.

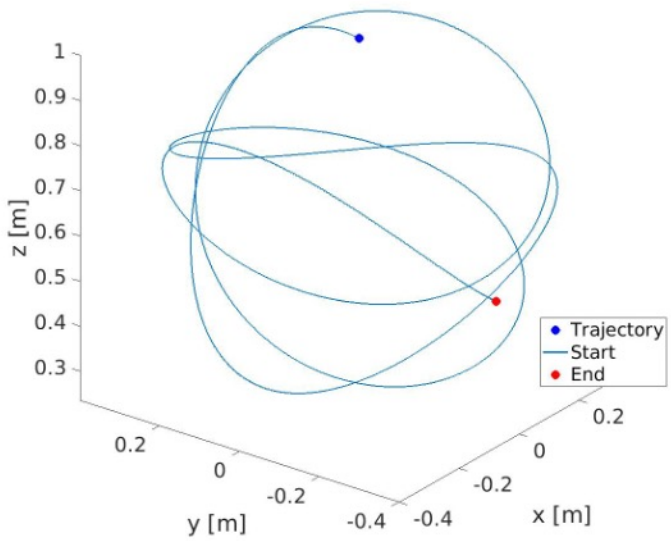

Fig. 11 COMMANDS calibration trajectory performed on STAR

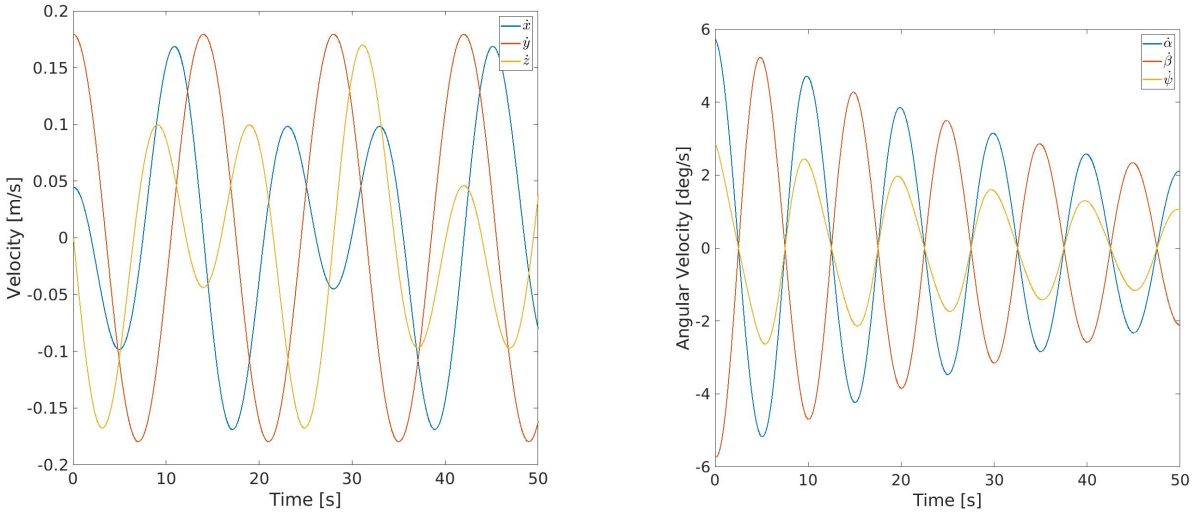

(a) Translational velocity

(b) Angular velocity

Fig. 12 Velocity profiles for calibration trajectory performed on STAR

B. Velocimeter LIDAR-Based Terrain Relative Navigation

The first official STAR test campaign was designed to asses velocimeter LIDAR-based pose estimation algorithms in the context of terrain relative navigation. The novel velocimeter LIDAR yields point-wise relative position and Doppler velocity measurements for every pixel in its field-of-view at 10 Hz. It was shown that leveraging relative Doppler velocity distributions generally yields more confident state estimates than standard 3D feature-based navigation filters in [9, 14]. However, this test was devised to evaluate the robustness of said pose estimation algorithm in a more dynamic scenario. Four different trajectories were generated to emulate various EDL situations including a simple 1D vertical descent, a 3D diagonal traverse, an inclined decelerating 'reentry' trajectory, and an oscillatory trajectory to emulate a body under parachute. The position, translational velocity, orientation, and rotational velocity profiles for all four

trajectories are displayed in Fig. 13. Note that in some of the sub-figures of Fig. 13, trajectories that cannot be observed are coincident with the observable trajectory.

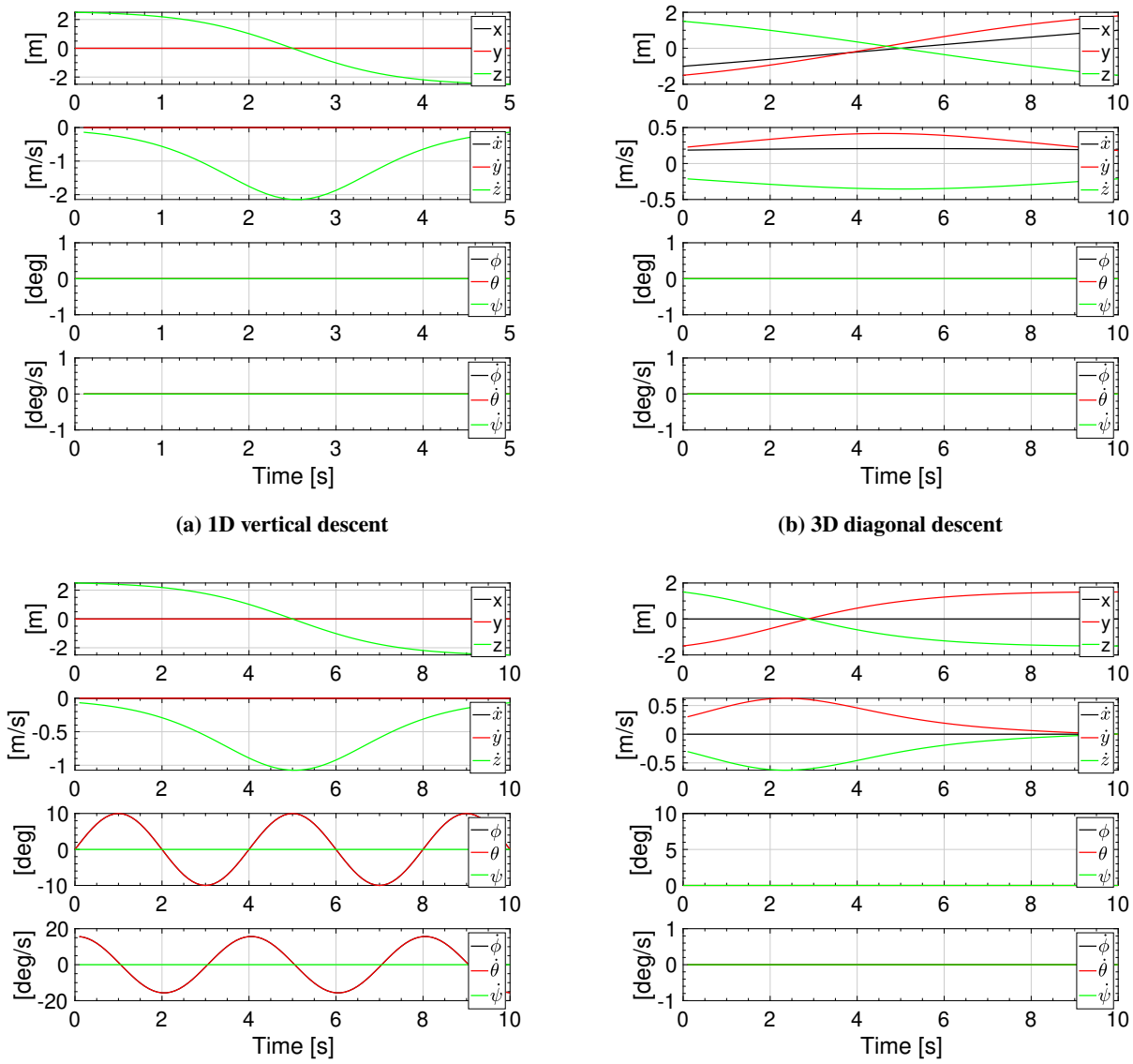

(a) 1D vertical descent

(b) 3D diagonal descent

(c) Emulated descent under parachute

(d) Emulated inclined reentry

Fig. 13 Trajectory profiles for STAR testing campaign

The custom designed payload that was mounted to the STAR end-effector consisted of the velocimeter LIDAR, an Intel NUC and a VectorNav VN-200T IMU, and is displayed in Fig. 14. The homogeneous transformations mapping the IMU to the LIDAR, and the IMU to the OptiTrack body frame were obtained via a perspective-n-point solution using a calibration checkerboard. Upon initialization of the velocimeter LIDAR, IMU, and OptiTrack motion capture system data stream, the robot performed the desired trajectory and all data was recorded for post-processing.

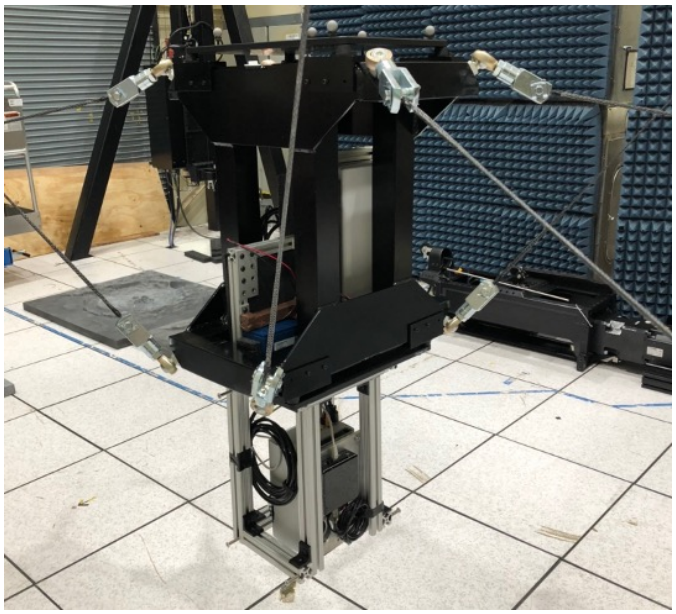

Fig. 14 Custom designed enclosure for velocimeter LIDAR, Intel NUC, and VectorNav VN-200T IMU mounted on STAR end-effector

Previous researchers in the Aeroscience and Flight Mechanics division (EG) at JSC developed 13 high resolution 4'×4'×4" topographical tiles of well known lunar sites to be used as mock terrains for emulating lunar EDL scenarios. The tiles directly represent specific lunar locations, such as the Hesiodus and Copernicus craters as displayed in Fig. 15. However, the elevation data, originally gathered during the Lunar Reconnaissance Orbiter (LRO) and Lunar Orbiter Laser Altimeter (LOLA) missions, was exaggerated to provide enough height disparity to enable surface analysis and reconstruction with LIDAR sensors. These tiles were air brushed to exhibit hill-shading given a specific solar illumination conditions. The shading was intended to imitate the terrain surface albedo and to create consistent artificial shadows produced by craters and ridges. Thus, the tiles contain abundant unique 'features' that can be detected, characterized, and tracked by 2D machine vision based navigation algorithms.

(a) Hesiodus A crater **(b) Copernicus crater**

Fig. 15 4'×4' mock lunar terrain tiles

All of the mock lunar terrain tiles were placed on the floor below the STAR end-effector, as displayed in Fig. 16. The tiles were also outfitted with several retro-reflective markers to artificially create predefined 'landmarks' which the velocimeter LIDAR could reliably detect. The configuration of these markers was calibrated and stored in a database which could be referenced by a feature correspondence algorithm.

Fig. 16 Lunar tiles placed beneath STAR end-effector

Figs. 17-20 display the resultant position and velocity state error and 3σ bounds yielded by the Doppler LIDAR-informed MEKF for the vertical descent, diagonal descent, inclined reentry descent, and emulated parachute descent, respectively. For space considerations, the entirety of these results will not be discussed in detail, as the technicalities of navigation filtering lie outside the scope of this work. However, it is important to note that the results from this test campaign substantiate the claims made in [9] that velocimeter LIDARs can reliably and accurately obtain attitude, position, and velocity state estimates in highly dynamic and uncertain environments. All state error trajectories lie within their 3σ bounds indicating a consistent navigation filter.

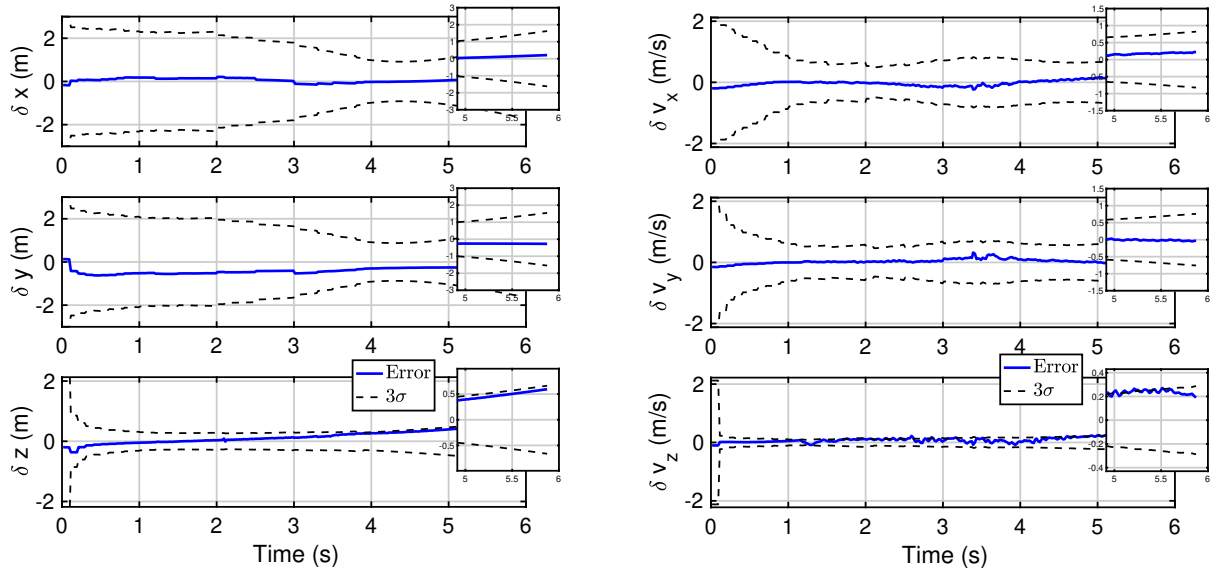

(a) Position error and 3σ standard deviation error bounds **(b) Velocity error and 3σ standard deviation error bounds**

Fig. 17 Velocimeter LIDAR-based MEKF performance for vertical descent

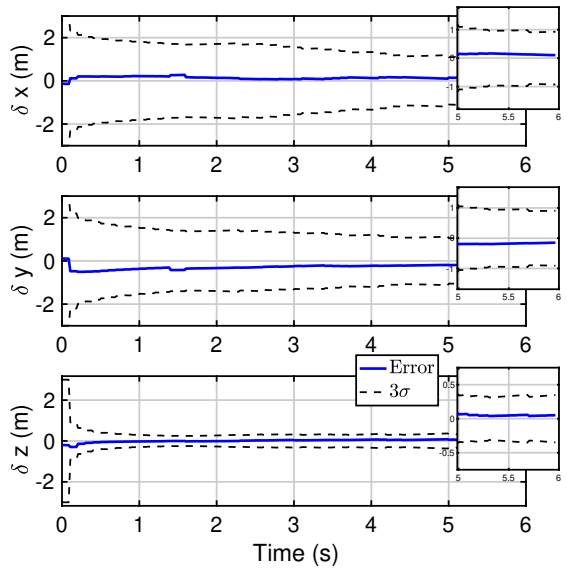

(a) Position error and 3σ standard deviation error bounds

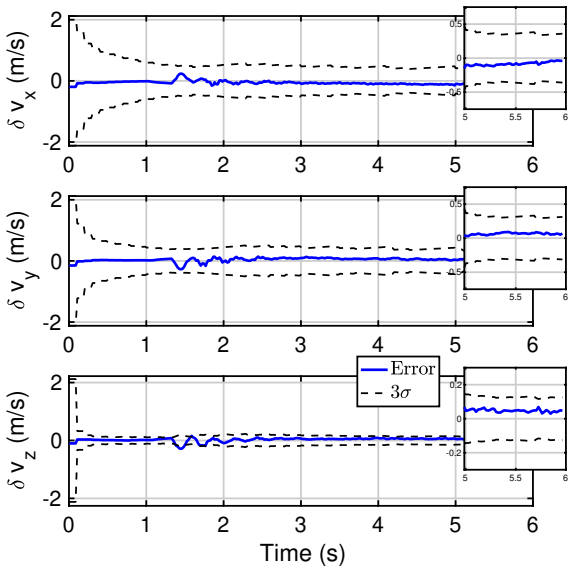

(b) Velocity error and 3σ standard deviation error bounds

Fig. 18 Velocimeter LIDAR-based MEKF performance for diagonal descent

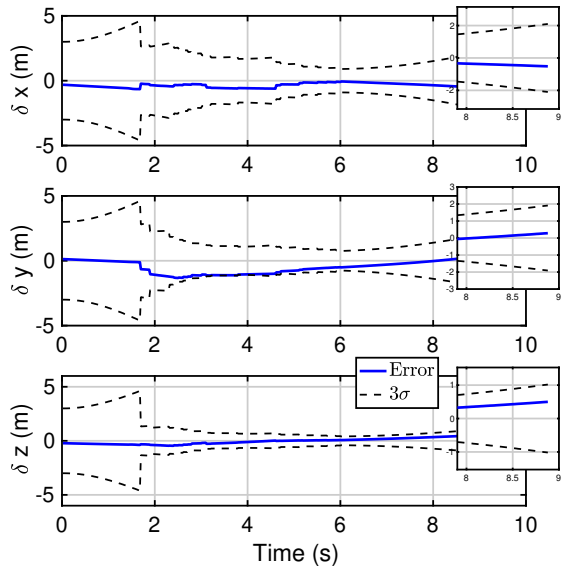

(a) Position error and 3σ standard deviation error bounds

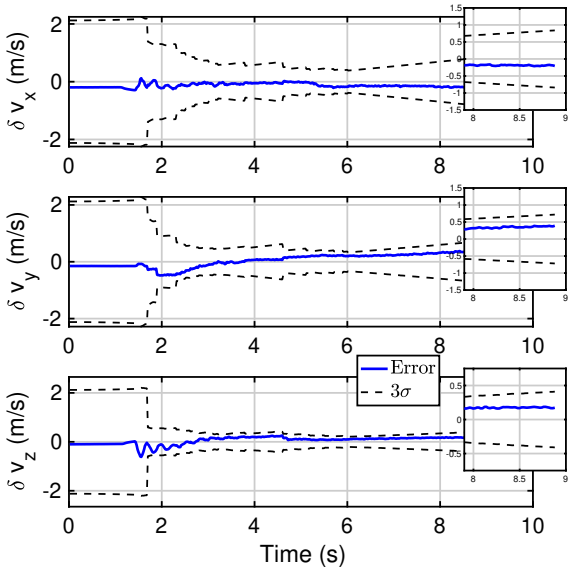

(b) Velocity error and 3σ standard deviation error bounds

Fig. 19 Velocimeter LIDAR-based MEKF performance for inclined 'reentry' descent

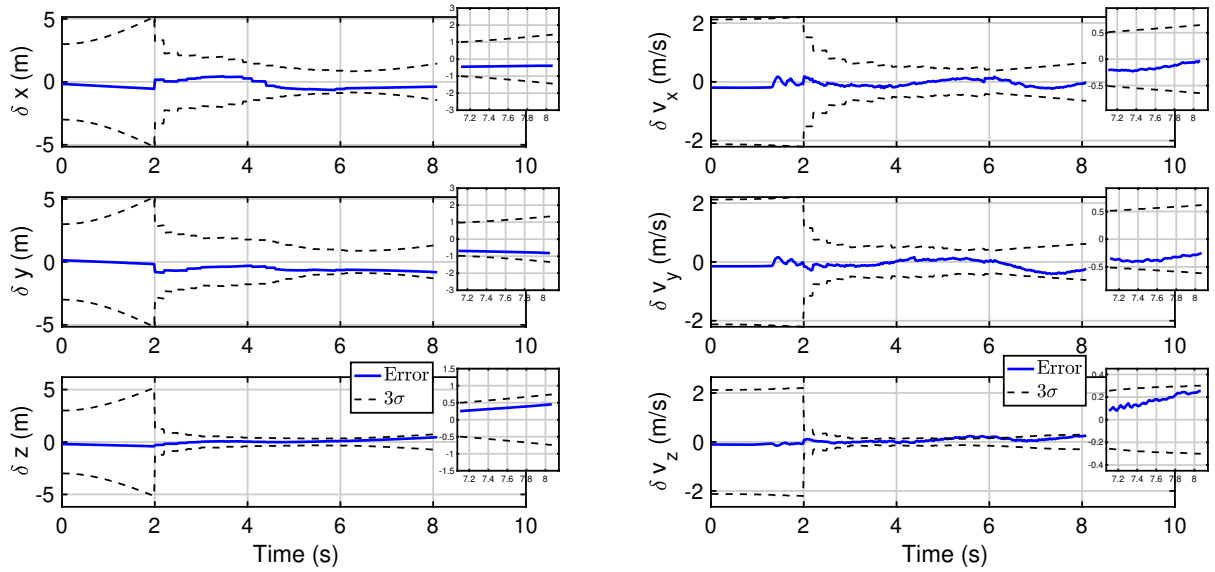

(a) Position error and 3σ standard deviation error bounds **(b) Velocity error and 3σ standard deviation error bounds**

Fig. 20 Velocimeter LIDAR-based MEKF performance for emulated parachute descent

C. Astrobotic UltraNav HWIL Testing

To fulfill Astrobotic's UltraNav SBIR project objectives and evaluate the efficacy of UltraNav's real-time performance, a team of Astrobotic researchers visited NASA JSC to perform HWIL testing with STAR. The overarching goal of this test campaign was to verify the hardware/software interfaces in a dynamic environment and evaluate Astrobotic's proprietary 2D machine vision-based pose estimation algorithm in the context of terrain relative navigation. UltraNav consists of a high-quality compact camera and accompanying computer and electronic components utilizing a proven suite of accelerated computer vision algorithms [15]. During operation, UltraNav acquires images, detects/classifies 2D features, and attempts to correspond the set of observed features with a stored database to yield a pose estimate. The Astrobotic team laid out several printed lunar maps which were created based on the Kaguya mission's publicly available digital elevation map (DEM) data products and seamless terrain camera (TC) images. The DEMs and TC images were selected from a region in the northeastern hemisphere of the moon encompassing approximately 78.000°E to 82.500°E and 19.000°N to 24.000°N, as displayed in Fig. 21

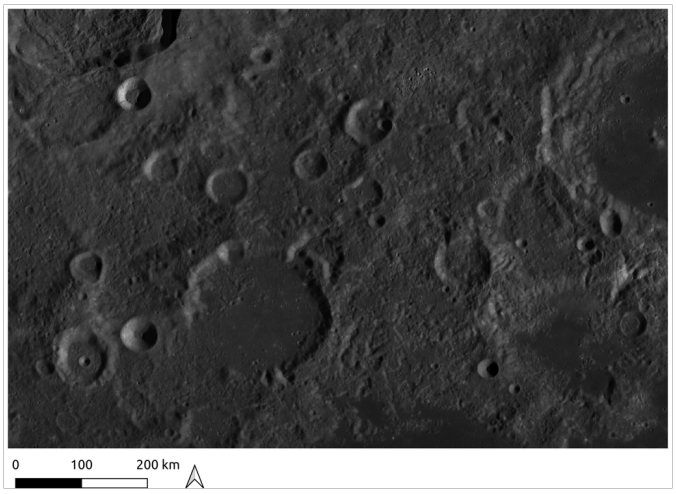

Fig. 21 Selected rgion of the lunar terrain to create TRN maps for STAR laboratory HWIL testing

The UltraNav payload directly attached to STAR's end-effector, as displayed in Fig. 22. The camera within the UltraNav sensor payload was calibrated prior to testing via Zhang's method of linear least squares. To emulate a lunar landscape, nine 2m×2m printed maps were placed on the floor of the STAR facility for UltraNav to image during testing, as displayed in Fig. 23. Each tile represented at 30km×30km lunar map at a resolution of 10 meters per pixel and was ortho-projected using the respective area's center point as the reference. Therefore, each tile was a 1:15,000 scale map.

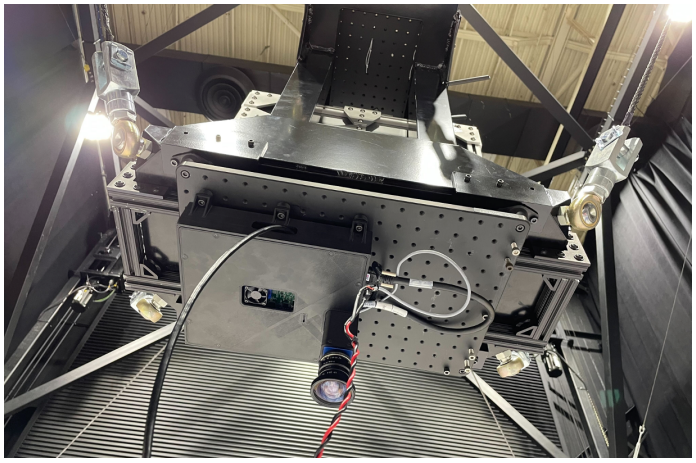

Fig. 22 UltraNav system attached to STAR's end-effector

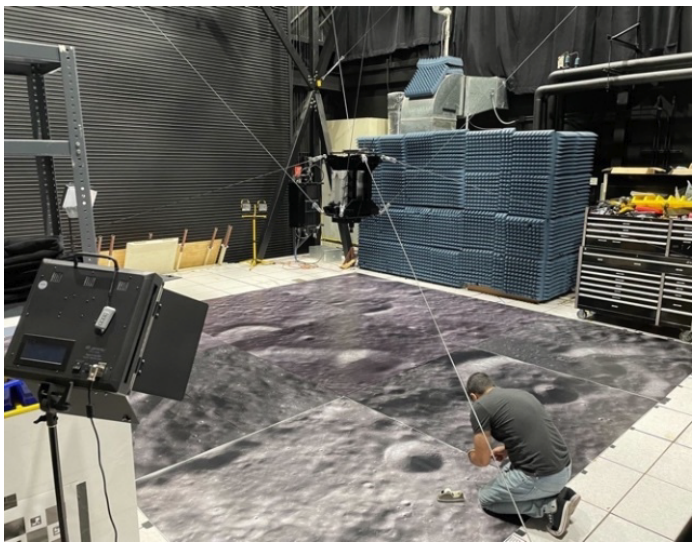

Fig. 23 Printed lunar maps placed on the ground within STARs operational area

The first test primarily aimed to evaluate the feature detection, identification, and matching algorithms. Several trajectories resembling a raster scan over each of the tiles were performed, as shown in Fig. 24. Note that Fig. 24 is represented in the scaled Cartesian space. This test specifically evaluated UltraNav's capability of correctly detecting which lunar tile was in direct view of the camera at any point in time. The raster trajectory consistently introduced "distractor" tiles into the field-of-view to increase the difficulty of the feature matching and tile retrieval algorithms. An example of the resultant feature correspondences provided by UltraNav is displayed in Fig. 25. UltraNav employed both local scale invariant feature transform (SIFT) and global vector of locally aggregated descriptor (VLAD) features to identify and characterize detected 2D features. Assuming the correct tile was identified, a pose estimate is then obtained by UltraNav expressed in the local lunar reference frame. The estimated position estimates and corresponding truth data obtained by Optitrack are displayed in Fig. 24

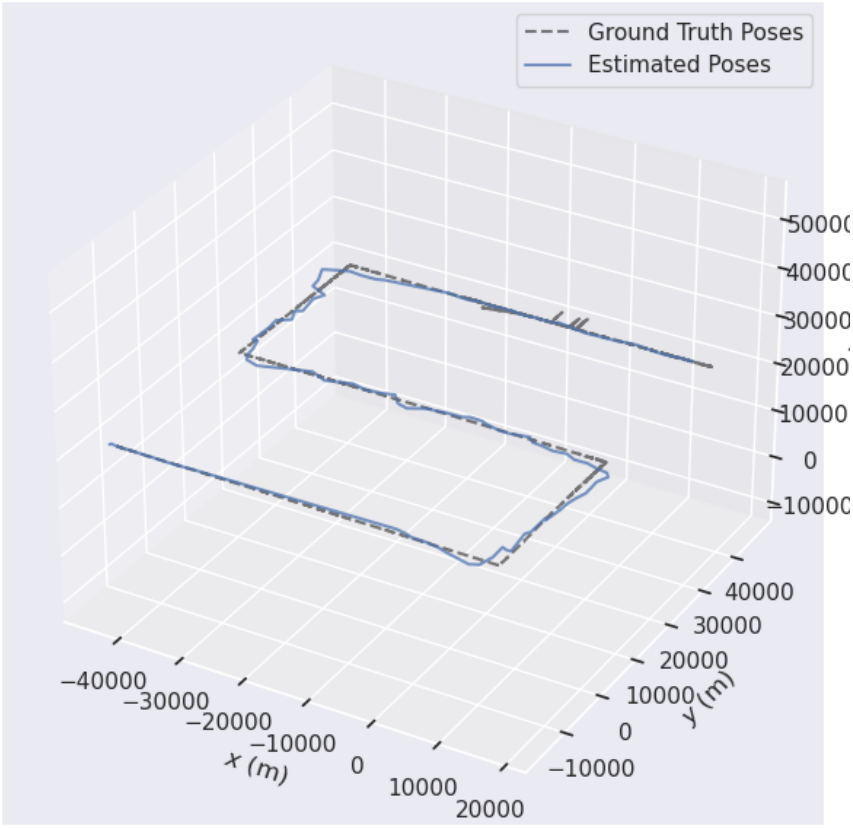

Fig. 24 Raster trajectory implemented by STAR to evaluate UltraNav's tile matching and pose estimation algorithms

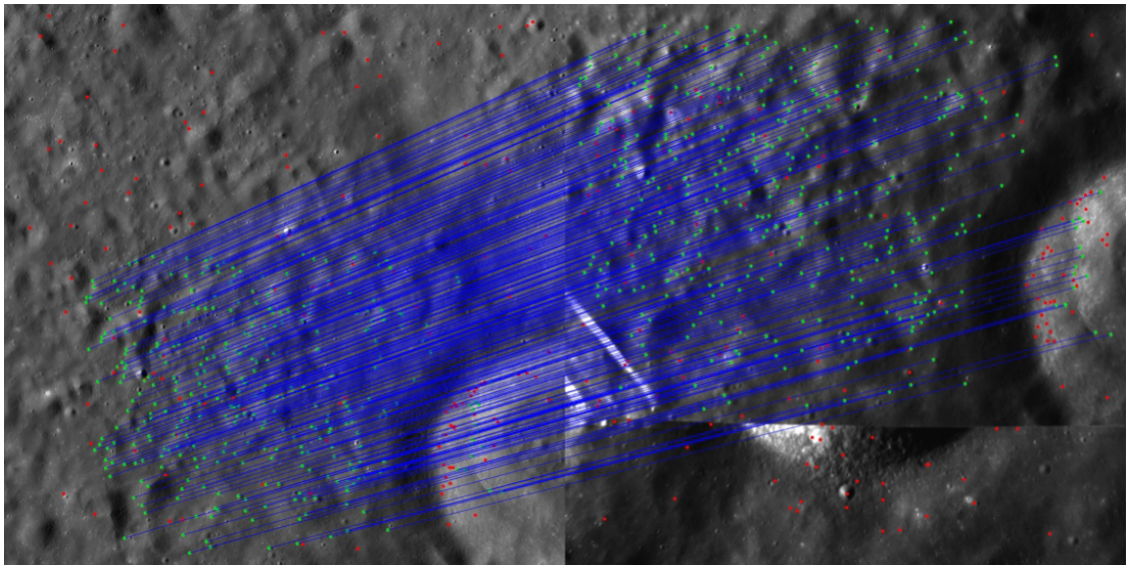

Fig. 25 Feature correspondences between (left) the selected TRN map from the on-board database and (right) the captured image

The second set of tests performed for this campaign focused on evaluating the accuracy of the pose estimation algorithm in a more realistic lunar descent environment. Instead of having nine tiles laid out in a discontinuous configuration, as done during the first test, five tiles were arranged to represent a continuous terrain, as shown in Fig. 26. UltraNav's pose estimation algorithm selected a "best" tile from the onboard database to match against and extract a navigation solution.

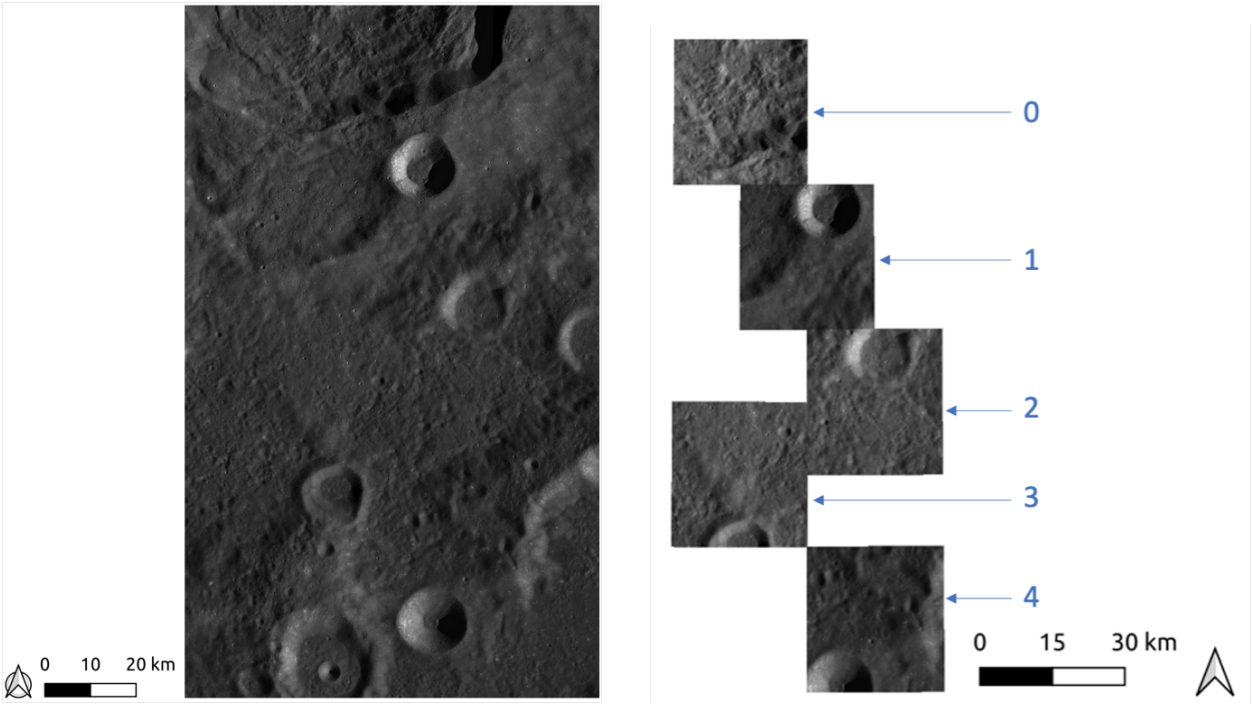

(a) **(b)**

Fig. 26 Lunar map configuration for the pose estimation test: (a) full lunar map (b) selected lunar tiles for testing

The second round of tests emphasized the consideration of spatial and time scales to emulate a realistic lunar descent. Data was collected for two different test trajectories emulating various portions of a Human Lander System (HLS) inspired lunar descent. Since the time scaling was true-to-life, the image acquisition rate was downsampled to 1 Hz to provide image overlap without excessive data redundancy. Fig. 27 displays the pose estimates plotted with the ground truth data for these two trajectories. The UltraNav experimental testing campaign with STAR successfully met its primary objective of demonstrating real-time functionality in a dynamic environment. UltraNav reliably detected features and generated valid and accurate pose estimates at high rates across the simulated descent trajectories. Preliminary Astrobotic analysis indicated that uncertainties in tile positions, noisy ground truth data yielded by OptiTrack, and slight discrepancies in the actual and commanded poses of STAR are the main contributors to the somewhat noisy estimated pose trajectories. These sources of noise were effectively amplified when scaling trajectories by 1:15,000.

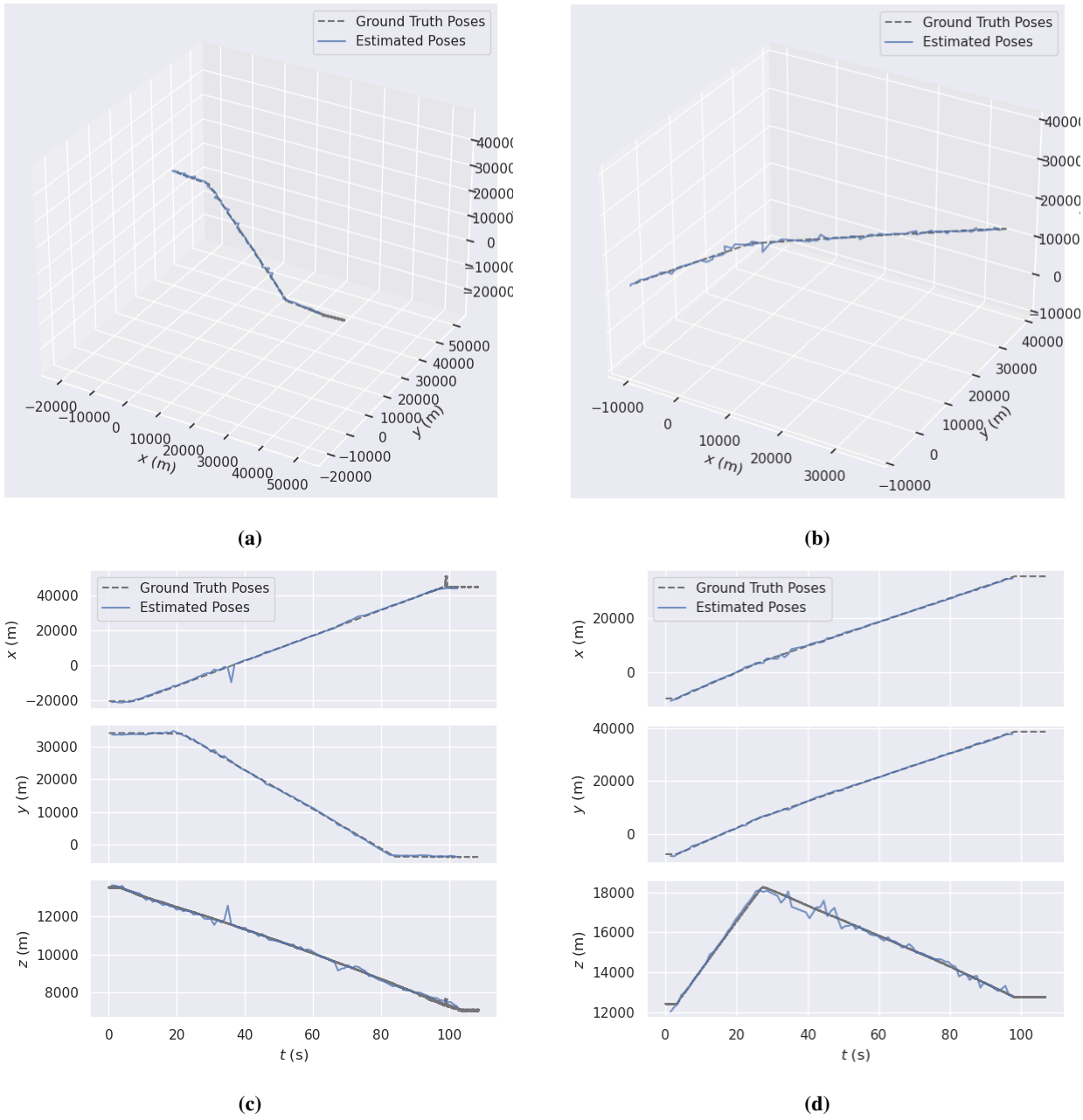

Fig. 27 Plots comparing UltraNav pose estimates and scaled ground truth data for (a,c) powered descent and (b,d) divert and descent trajectories

IV. Conclusions and Future Work

The novel 6-DOF motion emulation robot, STAR, was designed to enable HWIL testing of various spacecraft guidance, navigation, and control systems. This platform significantly aids in the rapid development and technology advancement of spacecraft GN&C systems which typically incur high costs associated with research and development due to inhibited access to realistic environmental testing. The STAR system features unrestricted 6-DoF motion emulation capability within the robot's operational envelope. STAR's parallel nature provides high stiffness and controllability for emulating arbitrary spacecraft motion.

Upon initial functional testing of STAR, two test campaigns were performed to demonstrate STARs unrestricted

motion emulation capability and modular payload support. The first test campaign was carried out with researchers from Texas A&M to evaluate the performance and robustness of a velocimeter LIDAR-based pose estimation algorithm. Previously developed, high-fidelity mock lunar terrain tiles were used to emulate a realistic planetary approach. Four different trajectories were employed to emulate various EDL scenarios. Test results bolstered previous claims stating that the velocimeter LIDAR-based navigation system can provide reliable and accurate pose estimates in highly dynamic and uncertain environments. STAR's second test campaign was carried out to verify the real-time performance of Astrobotic's UltraNav machine vision-based relative navigation system. Several 2D maps were developed by Astrobotic to mimic specific areas on the lunar surface. Upon image acquisition, UltraNav performed real-time 2D feature recognition, characterization, and matching to produce a correspondence to an image from the on-board database. The image comparison yields sufficient data to produce an instantaneous pose-estimate. For this test campaign, it was imperative to consider time and spatial scales so that the data obtained during testing would emulate the sensor output obtained during an actual lunar descent. Test results verified the real-time performance of UltraNav and provided baseline estimate error metrics.

Although STAR was originally developed to emulate EDL scenarios, the robot is agnostic to the commanded trajectory and the payload it is carrying. As a means to provide general navigation sensor data for any application, an internal sensor payload was developed that consists of a Cepton scanning LIDAR, a VectorNav VN-200T IMU, a FLIR Blackfly machine-vision camera, and an Intel NUC. This payload provides a real-time, time-synced data stream consisting of the output from the aforementioned sensors and a live-feed from the Optitrack motion capture system. The COMMANDS sensor payload was designed such that it will only output specified sensor data at specified rates. Thus, it stands as a utility for emulating wide ranges of spacecraft proximity operations and EDL scenarios.

The STAR lab is actively pursuing various relative spacecraft emulation and HWIL testing endeavors including several RPOD projects. Hardware to emulate multi-body relative motion operations is currently under-development. RPOD-related projects including covariance-constrained feedback control for docking and autonomous in-space assembly and manufacturing are also underway. Further, researchers at the STAR lab are currently developing 3D lunar tiles with larger elevation relief to enable higher-fidelity surface reconstruction and 3D-feature tracking algorithms to be tested. New lighting solutions will also be developed to enable variable illumination conditions during testing. These improvements pave the way for unprecedented capabilities in 6-DoF motion emulation to support future ventures to the Moon and beyond.

References

[1] Jairala, J. C., Durkin, R., Marak, R. J., Sipila, S. A., Ney, Z. A., Parazynski, S. E., and Thomason, A. H., "EVA Development and Verification Testing at NASA's Neutral Buoyancy Laboratory," *42nd International Conference on Environmental Systems (ICES)*, 2012.

[2] Sorge, R. N., "Space power facility-capabilities for space environmental testing within a single facility," *Space Simulation Conference*, 2013.

[3] Regehr, M. W., Acikmese, A. B., Ahmed, A., Aung, M., Clark, K., MacNeal, P., Shields, J., Singh, G., Bailey, R., Bushnell, C., et al., "The formation control testbed," *2004 IEEE Aerospace Conference Proceedings (IEEE Cat. No. 04TH8720)*, Vol. 1, IEEE, 2004, pp. 557–564.

[4] Valle, P., "Reduced gravity testing of robots (and humans) using the active response gravity offload system," *International Conference on Intelligent Robots and Systems*, 2017.

[5] Peck, C., Adams, D. W., McElreath, J., Verras, A., Hiemerl, J., Majji, M., Benedict, M., and Junkins, J., "Autonomous Deployment of Payload Packages to Spinning Rocket Bodies: Approach, Apparatus, and Emulation Using Ground Robotics," *Advances in the Astronautical Sciences*, Vol. 172, 2020.

[6] Adams, D., and Majji, M., "Velocimeter LIDAR-Based Relative Rate Estimation for Autonomous Rendezvous, Proximity Operations, and Docking Applications," *44th annual AAS Guidance, Navigation and Control Conference*, 2022.

[7] Carson, J. M., Munk, M. M., Sostaric, R. R., Estes, J. N., Amzajerdian, F., Bryan Blair, J., Rutishauser, D. K., Restrepo, C. I., Cianciolo, A. D., Chen, G. T., and Tse, T., "The splice project: Continuing nasa development of gnc technologies for safe and precise landing," *AIAA Scitech 2019 Forum*, , No. January, 2019, pp. 1–9. https://doi.org/10.2514/6.2019-0660.

[8] Sostaric, R. R., Pedrotty, S., Carson, J. M., Estes, J. N., Amzajerdian, F., Dwyer-Cianciolo, A. M., and Blair, J. B., "The SPLICE Project: Safe and Precise Landing Technology Development and Testing," *AIAA Scitech 2021 Forum*, 2021. URL https://arc.aiaa.org/doi/abs/10.2514/6.2021-0256.

[9] Adams, D., Peck, C., and Majji, M., "Velocimeter LIDAR-Based Multiplicative Extended Kalman Filter for Terrain Relative Navigation," *AIAA Scitech 2022 Forum*, 2022.

[10] Stanford Artificial Intelligence Laboratory et al., "Robotic Operating System," , 2018. URL https://www.ros.org.

[11] Moore, M., Sooknanan, J., and Holley, J., "Bobble-Bot: An educational platform for real-time control with ROS," *2019 IEEE International Symposium on Measurement and Control in Robotics (ISMCR)*, 2019, pp. B3–2–1–B3–2–7. https://doi.org/10.1109/ISMCR47492.2019.8955713.

[12] NASA, "Trick," , 2015. URL https://github.com/nasa/trick.

[13] Ramos, J. H., Brink, K. M., Ganesh, P., and Hurtado, J. E., "Factorized Partial-Update Schmidt–Kalman Filter," *Journal of Guidance, Control, and Dynamics*, Vol. 45, No. 9, 2022, pp. 1567–1582. https://doi.org/10.2514/1.G006449, URL https://doi.org/10.2514/1.G006449.

[14] Adams, D., Majji, M., Stevens, S. U., Kulkarni, T., Katake, A., San Martin, A., and Skulsky, E., "Velocimeter LIDAR Based Bulk Velocity Estimation for Terrain Relative Navigation Applications," *AIAA Scitech 2022 Forum*, 2022.

[15] Astrobotic, "Astrobotic Awarded NASA Contract to develop UltraNav smart camera for next-generation space missions," , 2020. URL https://www.astrobotic.com/astrobotic-awarded-nasa-contract-to-develop-ultranav-smart-camera-for-next-generation-space-missions/.